IEEE Access
Multidisciplinary | Rapid Review | Open Access Journal

Received 1 September 2026, accepted 15 September 2026, date of publication 22 September 2026,
date of current version 28 September 2026.

Digital Object Identifier 10.1109/ACCESS.2026.3736005

RESEARCH ARTICLE

Deep-Learning-Based Interference-Mitigation Method Using Null-Space Beamforming for Hybrid-Array

JAEHYUK LIM [1], (Member, IEEE), SEUNGHYUN JANG [1], (Member, IEEE), HOGEUN YOO [2], AND JAEHOON LEE [2]

[1]Terrestrial and Non-Terrestrial Integrated Telecommunications Research Laboratory, Electronics and Telecommunications Research Institute (ETRI), Daejeon 34129, Republic of Korea
[2]Department of Computer Science and Engineering, Korea University, Seoul 02841, Republic of Korea

Corresponding author: Jaehoon Lee (ejhoon@korea.ac.kr)

This work was supported by the Institute of Information and Communications Technology Planning and Evaluation (IITP) grant funded by Korean Government (MSIT), Development of Technologies for Integrating Radio-Based Sensing and Communication, and a Base Station Prototype, under Grant RS-2026-25525599.

ABSTRACT Deep-learning-based beamforming methods for spatial-domain interference rejection have been developed for fully digital arrays and cannot be directly applied to the partially-connected hybrid analog–digital architectures commonly used in large-aperture radar systems. We propose a hybrid array deep neural network-based null-space beamformer (HA-DNN-NSB), which extends the DNN-NSB framework to a partially connected hybrid uniformly spaced linear array. We first derive the mathematical formulation for null-space beamforming (NSB) for the hybrid array structure and prove that both the autocorrelation matrix and optimal weights depend solely on relative steering vectors. Building on this property, we introduce a steering angle normalization technique that aligns the analog beamformer with the desired signal direction, yielding a theoretical SINR improvement over the hybrid array NSB without steering angle normalization and resolving the interference-to-signal ratio (ISR) dependency that limits conventional DNN-NSB when the desired and interfering signals have comparable power levels. The proposed HA-DNN-NSB directly infers the digital beamforming weights from the angle-normalized autocorrelation matrix through a fully connected DNN, without requiring prior interference information. Simulation results showed that, under a fixed hybrid configuration, the proposed method maintained near-optimal SINR across the entire ISR range, whereas conventional DNN-NSB exhibited catastrophic failure at ISR $\approx$ 0 dB. Across varying RF chain configurations, HA-DNN-NSB consistently achieved near-optimal SINR performance regardless of the number of RF chains, whereas the recurrent neural network-based counterpart exhibited a performance plateau and failed to exploit the additional spatial degrees of freedom provided by more RF chains. These results confirmed the effectiveness of the proposed HA-DNN-NSB as a practical deep-learning-based beamforming solution for hybrid-array radar systems.

INDEX TERMS Deep neural network, hybrid array, interference mitigation, null-space beamforming, steering angle normalization.

I. INTRODUCTION

In modern radar systems, adaptive beamforming plays a central role in suppressing interference signals while maintaining the reception of desired signals. With rapid advances in deep learning (DL), researchers have increasingly explored DL-based approaches to beamforming weight generation, aiming to replace or augment conventional methods such as minimum variance distortionless response (MVDR) and null-space beamforming (NSB). These efforts span a broad

The associate editor coordinating the review of this manuscript and approving it for publication was Xuebo Zhang.

© 2026 The Authors. This work is licensed under a Creative Commons Attribution 4.0 License.
For more information, see https://creativecommons.org/licenses/by/4.0/

range of topics including DL-based direction-of-arrival (DOA) estimation [1], [2], [3], [4], [5], [6], [7], anti-jamming strategies using reinforcement learning [8], [9], [10], [11], [12], radar resource management [13], [14], [15], [16], and direct beamforming weight inference from received signals [17], [18], [19], [20], [21], [22].

Despite significant progress, the cost and power consumption of large-aperture antenna arrays, which are essential for high-gain radar systems, are prohibitive when implemented with fully digital front-ends that dedicate a radio frequency (RF) chain to every antenna element. Hybrid analog–digital array architectures address this limitation by combining a reduced number of RF chains with analog beamforming networks. However, all DL-based beamforming methods for interference rejection [17], [18], [19], [20], [21] including the deep neural network-based null-space beamforming (DNN-NSB) method [22] assume fully digital architectures and cannot be directly applied to the hybrid array architecture. Meanwhile, DL-based beamforming for the hybrid architecture [23], [24], [25], [26], [27], [28], [29], [30] targets spectral efficiency in communication systems rather than spatial-domain interference suppression. Two slightly related studies exist [31], [32]; however, neither of them addresses direct beamforming weight generation for radar receiving systems. To the best of our knowledge, no prior work has tackled DL-based hybrid array receiving beamforming weight inference for spatial-domain interference rejection in radar systems. To address this, we propose the hybrid array DNN-NSB (HA-DNN-NSB), which extends the DNN-NSB framework [22] to hybrid array architectures. We first derive the mathematical formula for NSB for the hybrid array structure, proving that both the autocorrelation matrix and optimal weights depend solely on relative steering vectors. Based on this theoretical foundation, we introduce a steering angle normalization (SAN) technique that resolves the interference-to-signal ratio (ISR) dependency inherent in conventional DNN-NSB when the desired signal and interference have comparable power levels. Unlike the existing DL-based hybrid beamforming methods [23], [24], [25], [26], [27], [28], [29], [30], which optimize the analog phase-shifter stage for communication objectives and do not use beam alignment as a normalization of the received autocorrelation matrix, SAN uses the alignment itself as an angular normalization of the received autocorrelation matrix. The resulting method enables direct weight inference from the reduced dimension hybrid observations without requiring prior knowledge of interference directions, representing the first DL-based approach for spatial-domain interference rejection in hybrid array configurations.

The remainder of this paper is organized as follows. Section II reviews related work on DL-based beamforming. Section III presents the signal model, hybrid configuration NSB formulation, and the theoretical analysis of SAN. Section IV describes the proposed HA-DNN-NSB architecture and training procedure. Section V provides experimental results and analysis. Section VI discusses the generalization and robustness of the proposed method. Finally, Section VII concludes the paper.

II. RELATED WORK

A. DL-BASED BEAMFORMING FOR INTERFERENCE REJECTION

DL-based beamforming for interference rejection has attracted growing attention owing to the limitations of conventional adaptive beamforming methods in complex scenarios. An early convolutional neural network (CNN)-based approach trained on MVDR-derived weights demonstrated interference rejection for a 10-element array, but was limited to only a single variable interference source and suffered from the inherent nonlinearity of MVDR when scaling to larger arrays [19]. A subsequent two-stage CNN-long short-term memory (CNN-LSTM) framework further extended the CNN-based approach to a 14-element array, estimating interferences and the desired signal with up to two variable interference sources; however, the method required prior knowledge of interference signal waveforms [20]. A complex-valued CNN further improved the CNN-based approach by directly processing the complex-valued covariance matrix for a 10-element array with two interference sources, demonstrating enhanced robustness under limited snapshot conditions compared to real-valued CNNs [21], while the scalability to larger arrays and more interferences remains to be investigated. In a different direction, a recurrent neural network (RNN) architecture with gated recurrent unit layers was employed to produce complex beamforming weights trained against NSB ground truth for up to 16 elements and 10 interferences [17]; however, the method relied on DOA estimation as input, increasing system complexity. More recently, a deep reinforcement learning (RL)-based adaptive nulling approach using the proximal policy optimization (PPO) algorithm was introduced for phased arrays under dynamic environments [18]; however, its effectiveness under more complex scenarios involving multiple interference sources has not been validated.

To address the scalability and prior-information requirements of these methods, the DNN-NSB method was proposed, which combines NSB with DL to directly infer beamforming weights from the autocorrelation matrix without requiring prior angle information [22]. By leveraging the inherently lower nonlinearity of NSB weights, whose complexity is governed by the number of interferences rather than array elements, DNN-NSB demonstrated near-optimum signal-to-interference-plus-noise ratio (SINR) performance with up to 32 array elements and up to four variable interference sources across different evaluation scenarios. However, DNN-NSB was developed exclusively for fully digital array configurations, which becomes impractical for large-array systems where cost and hardware complexity scale linearly with the number of RF chains. Moreover, DNN-NSB suffers from performance degradation when the desired signal and

TABLE 1. Parameter comparison of neural networks across studies and proposed model.

	Number of array elements	Number of interferences	Array architecture
[19]	10	1	Digital
[20]	14	2	Digital
[21]	10	2	Digital
[17]	16	10	Digital
[18]	10–50	1	Digital
[22]	8–32	4	Digital
HA-DNN-NSB	**32**	**4**	**Hybrid**

interference have comparable power levels (i.e., ISR ≈ 0 dB), as the autocorrelation matrix lacks power-based discriminative cues to distinguish between them. These limitations motivate the extension to hybrid array architectures with an angle normalization framework.

B. DL-BASED HYBRID CONFIGURATION BEAMFORMING IN COMMUNICATION SYSTEMS

In wireless communications, DL-based beamforming for hybrid array architecture has been extensively studied to reduce hardware complexity while maintaining communication performance. A DL-driven method was proposed for mmWave hybrid precoding [23], while subsequent studies addressed intelligent reflecting surface (IRS)-aided multiple-input multiple-output (MIMO) systems [24], wideband mmWave overhead minimization [25], and symbol-error probability minimization via deep unfolding [26]. Experience-driven approaches for massive MIMO [27] and graph neural network-based methods [28] have further advanced the field. Multi-agent deep RL [29] and unsupervised learning frameworks [30] have also been explored for hybrid beamforming optimization in multi-user scenarios. While these methods demonstrate the feasibility of DL-based hybrid beamforming, they are designed for fundamentally different objectives—primarily maximizing spectral efficiency, minimizing bit-error rates, or optimizing multi-stream transmission. They do not address the interference suppression requirements specific to radar systems, where the goal is to form precise nulls toward interference directions while maintaining gain toward the desired signal. The design criteria, signal models, and performance metrics differ substantially between communication and radar applications, precluding direct application of communication-oriented hybrid beamforming methods to radar interference rejection.

These observations reveal that no existing work addresses DL-based hybrid array beamforming weight generation for spatial-domain interference rejection in radar receiving systems, to the best of our knowledge. The main contributions of this study can be summarized as follows:

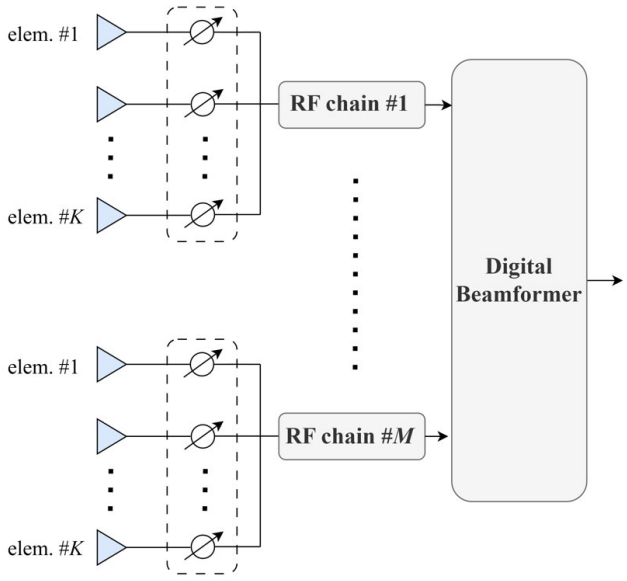

FIGURE 1. Structure of the partially-connected hybrid ULA with *N* antenna elements and *M* RF chains.

- Deriving the mathematical formulation for NSB for the hybrid array structure, establishing the theoretical foundation for applying NSB-based weight generation under the reduced dimension digital processing space imposed by the analog beamforming stage.
- Introducing a SAN technique that transforms both the autocorrelation matrix and optimal weights into functions of relative steering vectors alone, thereby resolving the ISR dependency that limits conventional DNN-NSB when the desired signal and interference have comparable power levels (i.e., ISR ≈ 0 dB).
- Proposing HA-DNN-NSB, which extends the fully digital DNN-NSB framework [22] to hybrid array architectures, representing the first DL-based method for direct beamforming weight inference targeting spatial-domain interference rejection in hybrid configurations.

Table 1 organizes the prior DL-based interference-rejection studies [17], [18], [19], [20], [21], [22] by the parameters that determine their applicability: the number of array elements, the maximum number of variable interferences handled, and the array architecture. The last column makes the position of the proposed method explicit: all prior DL-based interference-rejection studies assume a fully digital array, and the proposed HA-DNN-NSB is the only one operating on a hybrid architecture.

III. THEORY

A. SIGNAL AND HYBRID ARRAY MODEL

Fig. 1 illustrates the structure of the hybrid array antenna. At the front end, the system consists of N uniformly spaced linear array (ULA) elements. Unlike in the previous study [22], each received signal at the array elements passes through an analog phase shifter, and is partially connected

in groups of K, forming M that means the number of RF chains ($N = KM$). Finally, the signals are combined with M digital weight vectors $\boldsymbol{w} \in \mathbb{C}^{M\times 1}$, producing the overall output signal.

For the ULA, the steering vector $\boldsymbol{a}(\theta)$ is defined as

$$\boldsymbol{a}(\theta) = \left[\, 1 \;\cdots\; \exp(j\tfrac{2\pi}{\lambda} d(N-1)\sin(\theta)) \,\right]^T, \tag{1}$$

where λ is the signal wavelength, and d is typically set to $\lambda/2$ to prevent spatial aliasing. Then, the ULA signal vector $\boldsymbol{x_a}[i]$ can be defined as

$$\boldsymbol{x_a}[i] = s_d[i]\,\boldsymbol{a}(\theta_d) + \sum\nolimits_{q=1}^{Q} s_q[i]\,\boldsymbol{a}(\theta_q) + \boldsymbol{n}[i]. \tag{2}$$

where $s_d[i]$ and $s_q[i]$ are the desired and interfering signals, respectively; Q is the number of interferences, and $\boldsymbol{n}[i]$ represents additive noise. Also, θ_d and θ_q denote the DOA of the desired and interference signals. From (2), the received signal vector $\boldsymbol{x_r}[i]$ can be expressed as

$$\boldsymbol{x_r}[i] = \boldsymbol{F_{\mathbf{hybrid}}}^H \boldsymbol{x_a}, \tag{3}$$

where $\boldsymbol{F_{\mathbf{hybrid}}}$ can be expressed as

$$\boldsymbol{F_{\mathbf{hybrid}}} = diag(\boldsymbol{F}) \cdot \boldsymbol{\Lambda}. \tag{4}$$

Here, $\boldsymbol{F}$ is the analog-component vector of the phase shifters, that is, we transform $\boldsymbol{F} \in \mathbb{C}^{N\times 1}$ into $\boldsymbol{F_{\mathbf{hybrid}}} \in \mathbb{C}^{N\times M}$ to make $\boldsymbol{F}$ compatible with the hybrid structure. Also, $\boldsymbol{\Lambda} = \boldsymbol{I_M} \otimes \boldsymbol{1_K}$ where $\boldsymbol{I_M}$ is the $M \times M$ identity matrix and $\boldsymbol{1_k}$ is an all-ones vector of dimension $K \times 1$.

Assuming independence between $s_d[i]$, $s_q[i]$ and $\boldsymbol{n}[i]$ being i.i.d. complex Gaussian noise with variance σ_n^2, the autocorrelation matrix, $\boldsymbol{R_s}$ can be expressed as

$$\begin{aligned}\boldsymbol{R_s} = {} & \delta_d \boldsymbol{F_{\mathbf{hybrid}}} H \boldsymbol{a}(\theta_d)\,\boldsymbol{a}(\theta_d)^H \boldsymbol{F_{\mathbf{hybrid}}} \\ & + \sum\nolimits_{q=1}^{Q} \delta_q \boldsymbol{F_{\mathbf{hybrid}}} H \boldsymbol{a}(\theta_q)\,\boldsymbol{a}(\theta_q)^H \boldsymbol{F_{\mathbf{hybrid}}} + \sigma_n^2 \boldsymbol{I_M},\end{aligned} \tag{5}$$

where δ_d and δ_q denote the mean powers of the desired and interfering signals, respectively.

B. HYBRID ARRAY NULL STEERING BEAMFORMING

For a fully digital ULA with N elements, the NSB weights can be easily derived using the Lagrange multiplier method, as demonstrated in [17], [22]. The resulting weight vector $\boldsymbol{w}$ can be expressed as

$$\boldsymbol{w} = \boldsymbol{A}\left[\boldsymbol{A}^H \boldsymbol{A}\right]^{-1} \boldsymbol{g}, \tag{6}$$

where

$$\boldsymbol{A} = \left[\, \boldsymbol{a}(\theta_d)\; \boldsymbol{a}(\theta_1) \;\cdots\; \boldsymbol{a}(\theta_Q) \,\right], \tag{7}$$

$$\boldsymbol{g} = \left[\, 1\; 0 \;\cdots\; 0 \,\right]^T \tag{8}$$

Here, $\boldsymbol{A}$ contains the steering vectors corresponding to the desired and interfering signals, while $\boldsymbol{g}$ enforces unity gain in the desired direction and nulls in the interfering directions. This formulation is essentially the solution to the linear constraint $\boldsymbol{A^H w} = \boldsymbol{g}$, which directly enforces the desired beamforming pattern in the N-dimensional array space. However, this formulation cannot be directly applied to the hybrid array configuration. In the hybrid structure, the digital beamforming weights $\boldsymbol{w}$ operate in an M-dimensional space ($M < N$), while the physical steering constraints must be enforced in the N-dimensional array aperture through the combined analog-digital processing. Therefore, the constraint must be reformulated to account for the analog pre-processing stage $\boldsymbol{F_{\mathbf{hybrid}}}$. To obtain the optimal weights, we formulate the following constrained optimization problem:

$$min_{\boldsymbol{w}} \|\boldsymbol{w}\|^2 \;\; s.t.\, \boldsymbol{A}^H \boldsymbol{F_{\mathbf{hybrid}}} \boldsymbol{w} = \boldsymbol{g}. \tag{9}$$

The constraint $\boldsymbol{A}^H \boldsymbol{F_{\mathbf{hybrid}}} \boldsymbol{w} = \boldsymbol{g}$ ensures that the combined analog–digital beamforming maintains unity gain toward the desired signal and nulls toward interferences. Using the method of Lagrange multipliers, the hybrid array NSB weights $\boldsymbol{w}$ are obtained as

$$\boldsymbol{w} = \boldsymbol{F_{\mathbf{hybrid}}}^H \boldsymbol{A}(\boldsymbol{A}^H \boldsymbol{F_{\mathbf{hybrid}}} \boldsymbol{F_{\mathbf{hybrid}}}^H \boldsymbol{A})^{-1} \boldsymbol{g}. \tag{10}$$

In hybrid array configuration, a naive approach would fix the analog beamformer at a reference direction, for example, $\boldsymbol{F} = \boldsymbol{a}(0°)$. However, this causes analog gain loss. When the desired signal arrives from $\theta_d \neq 0°$, the fixed analog beam is misaligned, reducing the effective signal-to-noise ratio (SNR) at the digital beamformer input. To address this, we adopt SAN to (10), which adaptively aligns the analog beamformer with the desired signal direction, $\boldsymbol{F} = \boldsymbol{a}(\theta_d)$. This seemingly simple modification fundamentally transforms the beamforming geometry, as formalized through the following properties.

Property 1: The multiplication of the hybrid analog vector with the desired steering vector can be simplified as

$$\boldsymbol{F_{\mathbf{hybrid}}}^H \boldsymbol{a}(\theta_q) = \boldsymbol{\Lambda}^H \boldsymbol{a}^H(\theta_d)\boldsymbol{a}(\theta_q) = \boldsymbol{\Lambda}^H \boldsymbol{a'}(\Delta u_{d,q}), \tag{11}$$

where the relative steering vector is defined as

$$\boldsymbol{a'}(\boldsymbol{\Delta} u_{d,q}) = \left[\, 1 \;\cdots\; \exp(j\tfrac{2\pi}{\lambda} d(N-1)\Delta u_{d,q}) \,\right]^T, \tag{12}$$

with $\Delta u_{d,q} = \sin(\theta_q) - \sin(\theta_d)$. Using this property, the autocorrelation matrix $\boldsymbol{R_s}$ in (5) can be expressed in a simplified form as

$$\begin{aligned}\boldsymbol{R_s} = {} & \delta_d K^2 \boldsymbol{1_{M\times M}} + \sum_{q=1}^{Q} \delta_q \boldsymbol{\Lambda}\boldsymbol{\Lambda}^H \boldsymbol{a'}(\boldsymbol{\Delta} u_{d,q})\boldsymbol{a'}^H(\boldsymbol{\Delta} u_{d,q})\boldsymbol{\Lambda} \\ & + \sigma_n^2 \boldsymbol{I_M}.\end{aligned} \tag{13}$$

where $\boldsymbol{1_{M\times M}}$ is an all-ones matrix of dimension $M \times M$. Thus, the correlation matrix $\boldsymbol{R_s}$ is composed of: (i) a constant term δ_d associated with the desired signal, (ii) terms δ_q derived from the relative steering vectors of the interferences, and (iii) a noise term σ_n^2.

Property 2: For the steering matrix $\boldsymbol{A}$,the hybrid analog component leads to

$$\boldsymbol{F_{\mathbf{hybrid}}}^H \boldsymbol{A} = \boldsymbol{\Lambda}^H \boldsymbol{a}^H(\theta_d)\boldsymbol{A} = \boldsymbol{\Lambda}^H \boldsymbol{A}', \tag{14}$$

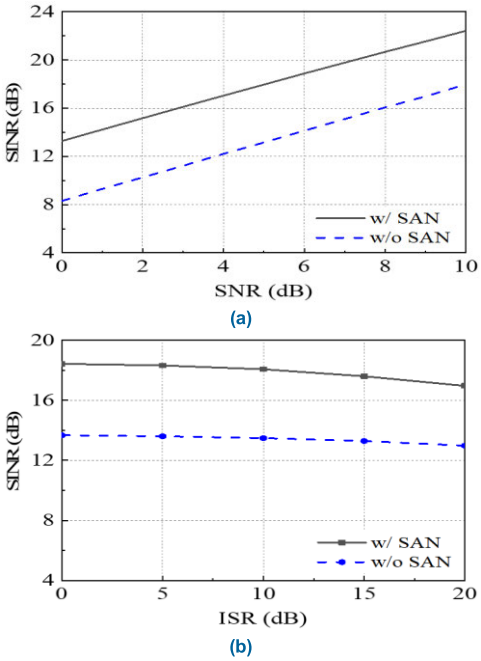

FIGURE 2. SINR performance comparison of hybrid array NSB without and with SAN: (a) SINR with respect to SNR, (b) SINR with respect to ISR.

where the relative steering matrix $\boldsymbol{A'}$ can be expressed as

$$\boldsymbol{A}' = \left[\, \mathbf{1}_N \; \boldsymbol{a'}(\Delta u_{d,1}) \cdots \boldsymbol{a'}(\Delta u_{d,Q}) \,\right]. \tag{15}$$

Substituting (14) in (10), the hybrid array NSB weights using the relative steering vectors, $\boldsymbol{w'}$,can be obtained as

$$\boldsymbol{w}' = \boldsymbol{\Lambda}^{\boldsymbol{H}} \boldsymbol{A}'(\boldsymbol{A}'\boldsymbol{H}\boldsymbol{\Lambda}\boldsymbol{\Lambda}^{\boldsymbol{H}}\boldsymbol{A}')^{-\mathbf{1}}\boldsymbol{g}. \tag{16}$$

In the hybrid structure, the autocorrelation matrix (13) and weights (16) are simplified into expressions that depend solely on the relative steering vectors; the autocorrelation matrix $\boldsymbol{R_s}$ and weights $\boldsymbol{w'}$ are governed by the same relative steering vector $\boldsymbol{a'}$. Therefore, the matrix $\boldsymbol{R_s}$ inherently contains all the information required to reconstruct the weights $\boldsymbol{w'}$ even under a hybrid configuration. Leveraging this property, our proposed approach directly infers the weights $\boldsymbol{w'}$ from the autocorrelation matrix $\boldsymbol{R_s}$ using a deep learning-based framework.

C. PERFORMANCE ANALYSIS OF THE SAN METHOD

Fig. 2 shows the SINR performance comparison between the hybrid array NSB weights without and with angle normalization, analytically computed using (10) and (16), respectively. In this simulation, the desired signal and interference angles were varied from $-40°$ to $40°$ in increments of $2°$, with $N = 32$, $M = 8$ and $Q = 4$. As shown in Fig. 2(a), the SAN-based weights demonstrated significant performance improvement in SINR across the entire SNR range, achieving an average gain of 4.76 dB for SNR values from 0 to 10 dB. This consistent improvement indicates that aligning the analog beamformer with the desired signal direction maintained optimal performance regardless of SNR conditions.

TABLE 2. Beamforming performance comparison without and with SAN.

	With SAN	Without SAN
Main lobe (°) [Mean/Std]	0.368 / 0.334	7.030 / 4.274
Null placement (°) [Mean/Std]	0.230 / 0.365	1.249 / 0.939
SINR (dB)	22.42	17.98

Fig. 2(b) illustrates the SINR performance with respect to ISR, where the SAN approach achieved an average improvement of 4.47 dB across ISR values from 0 to 20 dB. The performance gap remained relatively stable across different ISR conditions, confirming robustness in suppressing interference signals of varying interference power levels. The performance improvement originated from the adaptive alignment of the analog beamformer with the desired signal direction, which simultaneously improved both main lobe accuracy and null placement precision. As quantified in Table 2, the weights analytically computed with SAN reduced the main lobe pointing error from 7.030° to 0.368° and the null placement error from 1.249° to 0.230°. At a representative operating point (SNR = 5 dB, ISR = 10 dB), this collectively yielded a 4.44 dB SINR improvement.

Beyond performance improvements, SAN simplifies the theoretical framework for hybrid array beamforming. As shown in (13) and (16), the autocorrelation matrix and weight vector are expressed solely in terms of relative steering vectors $\boldsymbol{a'}$, eliminating the dependency on absolute angle information. This structural simplification is particularly critical for DL-based approaches. Without normalization, conventional DL-based beamforming methods [19], [22] fail when ISR = 0 dB because the neural network cannot distinguish between desired and interference signals based solely on their power levels. However, SAN resolves this limitation by consistently placing the desired signal at the center, while interference signals are represented by their relative angular positions. This geometric constraint enables direct weight inference from the autocorrelation matrix, even at ISR = 0 dB, as demonstrated in Section V.

IV. PROPOSED HA-DNN-NSB

We propose HA-DNN-NSB, a DNN-based beamformer for hybrid array architectures in which the deep neural network is trained to directly infer the hybrid array NSB weights $\boldsymbol{w'}$ from the autocorrelation matrix, as illustrated in Fig. 3. The proposed architecture consists of four stages. In the SAN stage, the ULA signal vector $\boldsymbol{x_a}$ is transformed into the received signal $\boldsymbol{x_r}$ by $\boldsymbol{F_{\text{hybrid}}}^{\boldsymbol{H}}(\theta_d)\,\boldsymbol{x_a}$, where the analog beamformer is aligned with the desired signal direction. In the preprocessing stage, the autocorrelation matrix is computed from $\boldsymbol{x_r}$ as $\boldsymbol{R_s} = \frac{1}{L}\sum \boldsymbol{x_r}\boldsymbol{x_r^H}$ with snapshots $L = 200$, and converted into the normalized input feature vector $\boldsymbol{z}$ for the DNN. In the

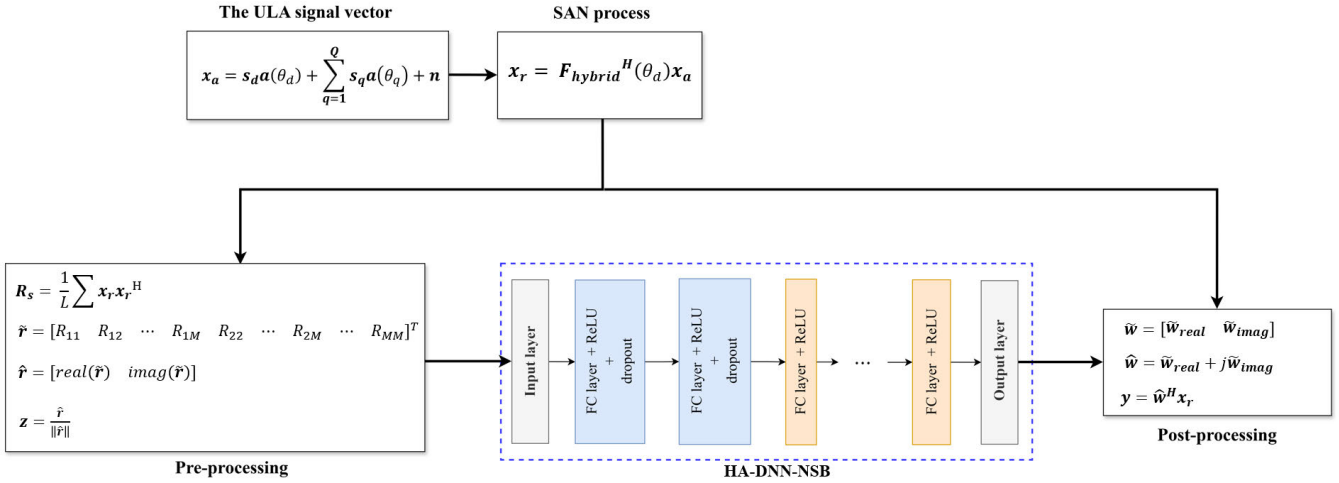

FIGURE 3. Architecture of the proposed HA-DNN-NSB beamformer.

DNN inference stage, the network maps the pre-processed autocorrelation matrix to the digital beamforming weights in the M-dimensional RF chain space, yielding the output $\tilde{\boldsymbol{w}}$. Finally, in the post-processing stage, the output signal vector $\boldsymbol{y}$ is obtained by applying the inferred weights $\hat{\boldsymbol{w}}$ to $\boldsymbol{x_r}$, that is, $\boldsymbol{y} = \hat{\boldsymbol{w}}^{\boldsymbol{H}}\boldsymbol{x_r}$ where $\hat{\boldsymbol{w}} = \tilde{\boldsymbol{w}}_{\boldsymbol{real}} + j\tilde{\boldsymbol{w}}_{\boldsymbol{imag}}$. The detailed pre-processing and post-processing procedures follow the methodology established in [22], adapted for the hybrid array configuration.

A. NETWORK CONFIGURATION

The proposed HA-DNN-NSB adopts a fully connected (FC) DNN architecture, as shown in Fig. 3. The network consists of L_h hidden layers, each followed by a rectified linear unit activation function. A dropout rate of 50% is applied to the first two FC layers to prevent overfitting. The input dimension is $M \times (M+1)$, derived from the real and imaginary parts of the upper triangular matrix of the $M \times M$ normalized autocorrelation matrix, and the output dimension is $2M$, representing the real and imaginary components of the complex-valued digital weight vector. The network depth and width are optimized through hyperparameter search for each hybrid array configuration.

B. TRAINING DATA GENERATION

Training data are generated by randomly sampling signal scenarios within specified parameter ranges. For all configurations, the number of antenna elements is fixed at $N = 32$, while the number of RF chains M varies according to the hybrid array configuration under evaluation. The desired signal direction θ_{d} and interference directions θ_{q} are uniformly sampled from the range $[-40°, 40°]$ independently in steps of 2°. The number of interference sources Q is varied from 1 to 4 for each evaluation scenario. The SNR is fixed at 5 dB, and ISR is uniformly sampled from 0 to 20 dB in steps of 5 dB. For each sampled scenario, the ground-truth weight vector $\boldsymbol{w'}$ is computed using (16), and the corresponding normalized autocorrelation matrix serves as the network input. A total of 1,200,000 training samples were generated. The network was trained using the Adam optimizer with MSE loss between the predicted and ground-truth normalized weight vectors. The complete set of training hyperparameters is summarized in Table 3.

TABLE 3. Simulation and training configuration.

Parameter	Value
Signal Configuration	-
Number of antenna elements (N)	32
Number of RF chains (M)	Scenario-dependent
Signal/interference angle range (θ_d, θ_q)	[−40°, 40°], 2° step
Number of interferences (Q)	1–4
SNR	5 dB
ISR range	0–20 dB, 5 dB step
Network Architecture	-
Hidden layers (L_h)	6
Neurons per hidden layer (H)	1,024
Dropout rate	0.5
Activation function	ReLU
Training Configuration	-
Total training samples	1,200,000
Optimizer	Adam
Initial learning rate	0.001
Learning rate drop period	2 epochs
Learning rate drop factor	0.8
Mini-batch size	1,024
Loss function	MSE
Number of epochs	100

V. EXPERIMENTAL RESULTS

A. SINR PERFORMANCE UNDER FIXED HYBRID CONFIGURATION

Fig. 4 presents the SINR performance comparison between four beamforming methods under the hybrid array structure ($M = 8$, $K = 4$) with four interferences ($Q = 4$):

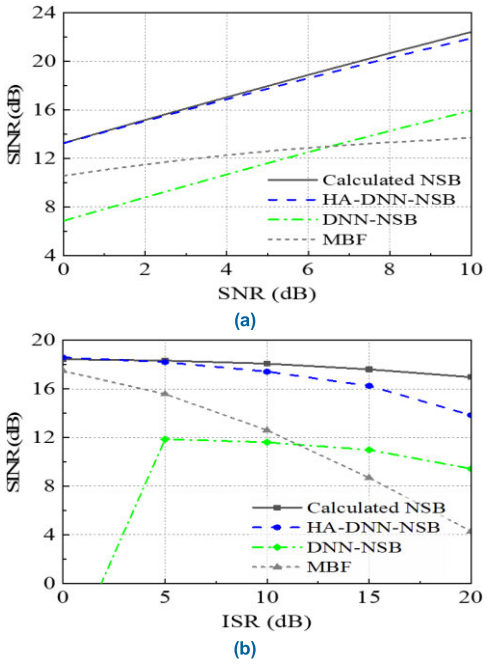

FIGURE 4. SINR performance comparison of calculated NSB, HA-DNN-NSB, DNN-NSB, and MBF under a fixed hybrid configuration ($M = 8$, $Q = 4$): (a) SINR with respect to SNR, (b) SINR with respect to ISR.

(i) calculated NSB, which computes the weights $\boldsymbol{w}'$ analytically using (16) with known interference directions, serving as the theoretical upper bound; (ii) the proposed HA-DNN-NSB, which combines SAN with DNN-based weight inference; (iii) DNN-NSB [22], which operates on a fully digital array ($N = M = 8$) without SAN; and (iv) matched beamforming (MBF), which applies SAN to the same hybrid array adopting a uniform weight vector ($\boldsymbol{w} = \mathbf{1}_M$), meaning that no adaptive null steering is performed toward interference directions. As MBF shares the same analog beamforming stage as HA-DNN-NSB, the performance gap between the two methods directly quantifies the gain from DNN-based adaptive null placement.

Fig. 4(a) shows the SINR with respect to SNR at a fixed ISR of 10 dB. The proposed HA-DNN-NSB closely followed the calculated NSB, ranging from 13 dB at SNR = 0 dB to 22 dB at SNR = 10 dB, while DNN-NSB exhibited a similar linear trend with a consistent offset of 6 dB below HA-DNN-NSB. This gap directly reflects the aperture advantage of the hybrid architecture: although both methods operate with the same number of RF chains ($M = 8$), HA-DNN-NSB leverages $N = 32$ physical elements through the analog beamforming network, whereas DNN-NSB is limited to $N = 8$ elements in its fully digital configuration. Compared to MBF, HA-DNN-NSB achieved a SINR improvement of 2.5 dB at SNR = 0 dB, increasing to 8.5 dB at SNR = 10 dB, confirming that DNN-based null steering provides increasingly effective interference suppression at higher SNR.

Fig. 4(b) presents the SINR with respect to ISR at a fixed SNR of 5 dB. A key observation concerns the behavior at ISR = 0 dB. DNN-NSB without SAN exhibited catastrophic failure at this operating point, yielding a SINR of −7 dB. This is attributed to the fact that, at ISR = 0 dB, the signal power contributions δ_d and δ_q in the autocorrelation matrix (5) become equal, rendering the desired and interference components structurally indistinguishable without prior angular information. Once ISR exceeded 0 dB, the power disparity provided partial discrimination, enabling recovery to 12 dB at ISR = 5 dB; however, performance remained substantially below that of the proposed method across all ISR conditions, partly owing to the aperture limitation of the smaller array aperture. In contrast, the proposed HA-DNN-NSB closely tracked the calculated NSB throughout the entire ISR range, achieving 18.5 dB at ISR = 0 dB and gradually decreasing to 14 dB at ISR = 20 dB. This result confirms that SAN resolves the ISR dependency by consistently centering the desired signal in the normalized angular domain, enabling reliable weight inference regardless of the power relationship between the desired signal and interferences. Although SINR gradually decreased at higher ISR, this was due to the finite null depth of the inferred weights, not a degradation in beamforming accuracy, as the main lobe pointing and null placement errors remained constant across ISR conditions.

The comparison with MBF further quantifies the contribution of DNN-based null steering. At ISR = 0 dB, the gap between HA-DNN-NSB and MBF was only 1 dB, indicating marginal benefit from null steering as interference power was low. As ISR increased, the gap widened substantially to 10 dB at ISR = 20 dB, where MBF degraded to 4 dB while HA-DNN-NSB maintained 14 dB. This confirmed that the null steering capability of DNN becomes essential as the interference environment intensifies.

B. PERFORMANCE COMPARISON WITH RESPECT TO THE NUMBER OF RF CHAINS

Fig. 5 presents the SINR performance with varying numbers of RF chains ($M = 4$, 8, 16, and 32) for $N = 32$ and $Q = 4$. To assess the advantage of the DNN architecture, we additionally evaluate HA-RNN-NSB, which replaces the DNN with an LSTM-based RNN architecture from [22] while retaining the same SAN and preprocessing pipeline. In Fig. 5, the upper row [(a)–(c)] shows SINR variation with respect to SNR (ISR = 10 dB), and the lower row [(d)–(f)] shows SINR variation with respect to ISR (SNR = 5 dB). Note that the SINR degradation observed with increasing ISR in (d)–(f) reflects the finite null depth rather than a deterioration in null placement accuracy, as confirmed by the constant main lobe pointing error and null placement error across ISR conditions.

Fig. 5(a) and (d) show the calculated NSB as the theoretical upper bound. As M increases from 4 to 32, the SINR improves consistently across both SNR and ISR ranges, reflecting the amount of spatial information preserved when reducing the N-dimensional array space to the M-dimensional digital processing space. When $M = 4$, the high compression

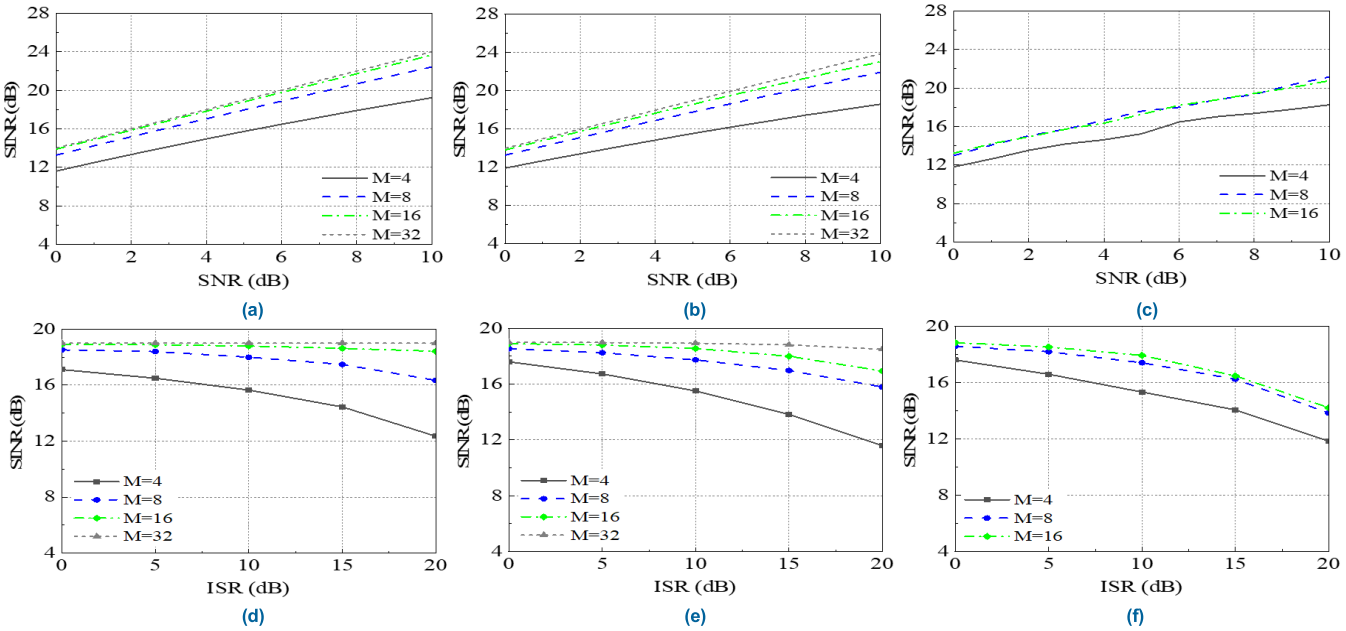

FIGURE 5. SINR performance with varying RF chain configurations ($M = 4, 8, 16, 32$; $N = 32$, $Q = 4$): SINR with respect to SNR for (a) calculated NSB, (b) HA-DNN-NSB, (c) HA-RNN-NSB, SINR with respect to ISR for (d) calculated NSB, (e) HA-DNN-NSB, (f) HA-RNN-NSB.

TABLE 4. Beamforming performance comparison of calculated NSB, HA-DNN-NSB, and HA-RNN-NSB Across RF Chain configurations.

	Calculated NSB			HA-DNN-NSB			HA-RNN-NSB		
M	4	8	16	4	8	16	4	8	16
Main lobe error (°) [Mean/Std]	1.099/1.232	0.368/0.334	0.093/0.135	1.092/1.210	0.300/0.266	0.069/0.086	0.812/0.900	0.299/0.253	0.167/0.236
Null placement error (°) [Mean/Std]	0.459/0.475	0.229/0.364	0.118/0.292	0.455/0.475	0.314/0.397	0.284/0.374	0.536/0.507	0.409/0.436	0.520/0.496
SINR (dB)	15.71	17.96	18.79	15.73	17.75	18.55	15.46	17.39	17.28

ratio ($N/M = 8$) leads to substantial spatial information loss and shallower null depth. In contrast, the configuration with $M = 8$ maintains a practically sufficient SINR level despite reducing the RF chains to one-quarter of the antenna elements. The configuration with $M = 16$ achieves SINR performance comparable to that of the fully digital case ($M = 32$), while the configuration with $M = 8$ offers a notable reduction in hardware cost at the expense of moderate SINR loss. Accordingly, a configuration with $M = 8$ or 16 represents a practical choice depending on cost and operational constraints. Fig. 5(b) and (e) show the HA-DNN-NSB performance across M values. The proposed method closely tracks the calculated NSB for all M values in both the SNR and ISR domains, with the SINR degradation slope under increasing ISR closely matching the theoretical bound. When $M = 16$ and 32, the curves are nearly indistinguishable from the upper bound. With $M = 4$ and 8, the lower absolute SINR is attributable to the reduced spatial information in the digital domain, not to degradation in the DNN inference accuracy. In contrast, Fig. 5(c) and (f) reveal clear limitations of the RNN architecture. When $M = 4$ and 8, HA-RNN-NSB achieves reasonable performance; however, it already exhibits a noticeable gap compared to HA-DNN-NSB, with steeper SINR degradation under increasing ISR. When $M = 16$, no meaningful SINR improvement over the case with $M = 8$ is observed despite the doubling of RF chains, indicating that the RNN architecture fails to exploit the additional degrees of freedom. When $M = 32$, the network fails to converge entirely during training. This scalability failure is attributed to the sequential processing nature of the RNN: as M increases, the input sequence length grows proportionally to $M \times (M+1)$, making it increasingly difficult to capture the long-range dependencies required for accurate weight inference.

Table 4 provides a quantitative comparison between calculated NSB, HA-DNN-NSB, and HA-RNN-NSB across three RF chain configurations ($M = 4$, 8, and 16). The calculated NSB reveals notable performance degradation when

TABLE 5. Computational complexity and processing time.

Method	Complexity	FLOPs	Processing time [s]
Calculated NSB	$O(M(Q+1)^2 + (Q+1)^3)$	2.60×10^3	0.090
HA-DNN-NSB	$O(DH + (L_h-1)H^2 + 2MH), D = M(M+1)$	1.07×10^7	0.0022
HA-RNN-NSB	$O(SL_rH^2), S = M(M+1)$	2.64×10^8	0.048
DNN-NSB [22]	$O(DH + (L_h-1)H^2 + 2NH), D = N(N+1)$	1.07×10^7	0.0022

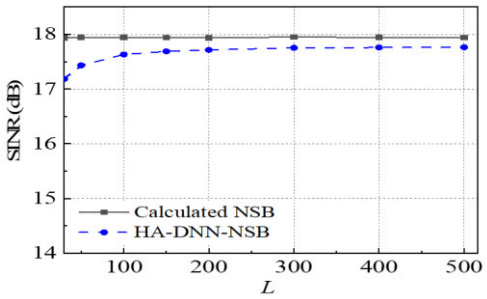

FIGURE 6. SINR performance comparison of calculated NSB and HA-DNN-NSB with respect to the number of snapshots, *L*.

$M = 4$ due to the limited spatial degrees of freedom. The main lobe pointing error increased to 1.099° compared to 0.368° for $M = 8$, and the null placement error rose to 0.459° compared to 0.229°, reflecting substantial spatial information loss in the digital processing space. Despite this inherent limitation, HA-DNN-NSB closely tracked the calculated NSB across all three configurations, achieving main lobe pointing errors of 1.092°, 0.300°, and 0.069° and SINR values of 15.73 dB, 17.75 dB, and 18.55 dB for $M = 4$, 8, and 16, respectively, with a maximum SINR gap of only 0.24 dB from the theoretical bound. In contrast, HA-RNN-NSB failed to exhibit consistent scaling. While comparable to HA-DNN-NSB for $M = 4$ and 8, the null placement error degraded from 0.409° for $M = 8$ to 0.520° for $M = 16$, and the SINR decreased from 17.39 dB to 17.28 dB despite the doubling of RF chains. These results demonstrate that HA-DNN-NSB provides consistent near-optimal performance with effective scalability, whereas the RNN architecture is unsuitable for hybrid array systems owing to its inability to benefit from increased RF chains. The results in Sections V-A and V-B substantiate three key advantages of the proposed HA-DNN-NSB. First, DNN accurately learned the mapping from the autocorrelation matrix to digital beamforming weights across all tested configurations, achieving near-optimal SINR with a maximum gap of only 0.24 dB from the calculated NSB. Second, SAN proved essential for hybrid array beamforming, both analytically and in the DL framework. It significantly improved the main lobe and null placement accuracy as analyzed in Section III-C, and resolved the ISR dependency that caused catastrophic failure at ISR = 0 dB in DNN-NSB without SAN. Third, the DNN architecture exhibited effective scalability with increasing RF chains, consistently improving SINR from $M = 4$ to 32, in contrast to the RNN architecture, which failed to benefit from additional degrees of freedom beyond $M = 8$. These findings confirm that HA-DNN-NSB provides a practical DL-based beamforming solution for hybrid array radar systems.

C. PERFORMANCE VERSUS THE NUMBER OF SNAPSHOTS

To examine the dependence on the number of snapshots, the model trained at $L = 200$ was evaluated over $L \in \{30, 50, 100, 150, 200, 300, 400, 500\}$ without any retraining (10^5 scenes per point; N = 32, M = 8, SNR = 5 dB, ISR = 10 dB), as shown in Fig. 6. The calculated NSB is unaffected by L, whereas the SINR of HA-DNN-NSB increases monotonically and saturates: the loss relative to the training condition is 0.5 dB at $L = 30$, 0.3 dB at $L = 50$, 0.1 dB at $L = 100$, and within 0.04 dB for L = 150 and above. Although $L = 300$, 400, and 500 lie outside the training condition, the SINR does not decrease and increases by a further 0.04 dB, which indicates that the model is not overfitted to $L = 200$. These results confirm that the proposed method is robust to the number of snapshots: a single model trained at $L = 200$ covers the entire range from $L = 30$ to $L = 500$ without retraining, with a maximum SINR loss of 0.5 dB.

D. COMPUTATIONAL COMPLEXITY AND PROCESSING TIME

The asymptotic complexity, the FLOP count required to generate one output weight vector, and the processing time for 3,000 inputs are summarized in Table 5. The processing times were measured on an NVIDIA RTX 5090 GPU for the learned methods and on a Ryzen 9 7950 × 3D CPU for the calculated NSB. The hybrid methods use $N = 32$, $M = 8$, $Q = 4$, whereas the fully digital DNN-NSB [22] uses $N = M = 8$ and $Q = 4$. HA-DNN-NSB and DNN-NSB use $H = 1024$ and $L_h = 6$, whereas HA-RNN-NSB uses $H = 256$, $L_r = 4$, and $S = 72$.

Based on these results, HA-DNN-NSB exploits a 32-element physical aperture while matching the computational requirements of the eight-element fully digital DNN-NSB; both require 1.07×10^7 FLOPs and 0.0022 s of processing time. In contrast, HA-RNN-NSB requires 24.8 times as many FLOPs and is approximately 22 times

TABLE 6. SINR under non-gaussian noise distributions.

Noise distribution	Calculated NSB [dB]	HA-DNN-NSB [dB]
Gaussian (reference)	17.96	17.74
Generalized Gaussian	17.96	17.74
Complex Student-t	18.04	17.82

slower because its recurrent weights are reused over $S = 72$ sequential steps. Although the calculated NSB has the lowest FLOP count, it has the longest measured processing time, 0.090 s, under the stated hardware settings because (16) requires a matrix inversion for every scene. Overall, HA-DNN-NSB replaces both the sequential recurrent computation of HA-RNN-NSB and the per-scene matrix inversion of the calculated NSB with a single forward pass.

VI. DISCUSSION

A. PERFORMANCE UNDER NON-GAUSSIAN NOISE

The additive term in (2) is spatially white thermal noise, so its non-Gaussian counterpart is impulsive, heavy-tailed noise. We therefore evaluated the trained model, without any retraining, under two standard parametric heavy-tailed models: the complex generalized Gaussian (GG) distribution with shape $\beta = 1$ (Laplacian) and the complex Student-t distribution with $\nu = 3$. All three distributions were matched to the same mean noise power so that only the tail behavior differs. The results at $N = 32$, $M = 8$, $Q = 4$, SNR $= 5$ dB, ISR $= 10$ dB are listed in Table 6. As shown in the table, the deviation across the three distributions is within 0.1 dB, and the gap between HA-DNN-NSB and the calculated NSB is unchanged by the noise distribution. This insensitivity is expected from the structure of the method. The network operates on the received autocorrelation matrix. Once the noise power is matched, the noise contribution to the ensemble autocorrelation matrix is $\sigma_n^2\mathrm{I}$ regardless of the tail shape, so the network input is unchanged in expectation. We therefore conclude that the proposed method is applicable to non-Gaussian noise without retraining.

B. ROBUSTNESS TO ANGLE MISMATCH

To assess SAN robustness, we introduced a bias $\varepsilon = 0°$ to $1.5°$ only in the estimated desired DOA and evaluated two configurations, $N = 32$, $M = 8$ and $N = 8$, $M = 4$. Both the calculated NSB and HA-DNN-NSB exhibited greater SINR degradation for $N = 32$ than for $N = 8$. At $N = 32$, HA-DNN-NSB showed a larger SINR loss than the calculated NSB, primarily in association with a larger main-lobe pointing error, while its null-placement accuracy remained comparable.

VII. CONCLUSION

We proposed HA-DNN-NSB, the first DL-based beamforming method for spatial-domain interference rejection in hybrid-array radar systems. Applying SAN to align the analog beamformer with the desired signal direction yielded a theoretical SINR improvement of 4.44 dB over the unnormalized hybrid array NSB, simultaneously reducing the main lobe pointing error and null placement error. The SAN formulation further revealed that the autocorrelation matrix and optimal weights depend solely on relative steering vectors, providing the structural condition under which DNN can directly infer the digital beamforming weights from the autocorrelation matrix without any prior interference information. Beyond beamforming accuracy, SAN resolved the ISR dependency that caused catastrophic failure of conventional DNN-NSB at ISR ≈ 0 dB, enabling robust operation across the entire ISR range.

The FC-DNN architecture also exhibited consistent scalability with increasing RF chains, achieving near-optimal SINR with a maximum gap of only 0.24 dB across $M = 4$, 8, and 16, whereas the RNN counterpart failed to benefit from additional degrees of freedom beyond $M = 8$. Of the evaluated configurations, $M = 16$ closely approached the fully digital upper bound, while $M = 8$ offered substantial hardware cost reduction with only moderate SINR loss, representing two practical operating points depending on cost and performance constraints. These results demonstrated that the proposed HA-DNN-NSB is an effective and practical DL-based beamforming solution for spatial-domain interference rejection in hybrid-array radar systems.

REFERENCES

[1] Y. Zhang, Y. Huang, J. Tao, S. Tang, H. C. So, and W. Hong, "A two-stage multi-layer perceptron for high-resolution DOA estimation," *IEEE Trans. Veh. Technol.*, vol. 73, no. 7, pp. 9616–9631, Jul. 2024, doi: 10.1109/TVT.2024.3368451.

[2] H. Xiang, B. Chen, M. Yang, and S. Xu, "Angle separation learning for coherent DOA estimation with deep sparse prior," *IEEE Commun. Lett.*, vol. 25, no. 2, pp. 465–469, Feb. 2021, doi: 10.1109/LCOMM.2020.3032733.

[3] Y. Cao, T. Lv, Z. Lin, P. Huang, and F. Lin, "Complex ResNet aided DoA estimation for near-field MIMO systems," *IEEE Trans. Veh. Technol.*, vol. 69, no. 10, pp. 11139–11151, Oct. 2020, doi: 10.1109/TVT.2020.3007894.

[4] L. Wu, Z.-M. Liu, and Z.-T. Huang, "Deep convolution network for direction of arrival estimation with sparse prior," *IEEE Signal Process. Lett.*, vol. 26, no. 11, pp. 1688–1692, Nov. 2019, doi: 10.1109/LSP.2019.2945115.

[5] M. Chen, Y. Gong, and X. Mao, "Deep neural network for estimation of direction of arrival with antenna array," *IEEE Access*, vol. 8, pp. 140688–140698, 2020, doi: 10.1109/ACCESS.2020.3012582.

[6] S. Xu, A. Brighente, B. Chen, M. Conti, X. Cheng, and D. Zhu, "Deep neural networks for direction of arrival estimation of multiple targets with sparse prior for line-of-sight scenarios," *IEEE Trans. Veh. Technol.*, vol. 72, no. 4, pp. 4683–4696, Apr. 2023, doi: 10.1109/TVT.2022.3224586.

[7] W. Liu, "Super resolution DOA estimation based on deep neural network," *Sci. Rep.*, vol. 10, no. 1, Nov. 2020, Art. no. 19859, doi: 10.1038/s41598-020-76608-y.

[8] Y. Jiang, Y. Yang, W. Zhang, and L. Guo, "Deep learning-based active jamming suppression for radar main lobe," *IET Signal Process.*, vol. 2024, no. 1, Jan. 2024, Art. no. 3179667, doi: 10.1049/2024/3179667.

[9] X. Li, J. Chen, X. Ling, and T. Wu, "Deep reinforcement learning-based anti-jamming algorithm using dual action network," *IEEE Trans. Wireless Commun.*, vol. 22, no. 7, pp. 4625–4637, Jul. 2023, doi: 10.1109/TWC.2022.3227575.

[10] H. Liu, H. Zhang, Y. He, and Y. Sun, "Jamming strategy optimization through dual Q-learning model against adaptive radar," *Sensors*, vol. 22, no. 1, p. 145, Dec. 2021, doi: 10.3390/s22010145.

[11] S. Zheng, C. Zhang, J. Hu, and S. Xu, "Radar-jamming decision-making based on improved Q-learning and FPGA hardware implementation," *Remote Sens.*, vol. 16, no. 7, p. 1190, Mar. 2024, doi: 10.3390/rs16071190.
[12] Z. Zhang, W. Yi, and Y. Yuan, "Reinforcement learning based agile transmission strategy for netted radar anti-jamming," in *Proc. IEEE Radar Conf. (RadarConf24)*, May 2024, pp. 1–6, doi: 10.1109/RadarConf2458775.2024.10548231.
[13] Z. Qu, Z. Ding, and P. Moo, "A machine learning radar scheduling method based on the EST algorithm," in *Proc. IEEE 18th Int. Conf. Cognit. Informat. Cognit. Comput. (ICCI*CC)*, Jul. 2019, pp. 22–27, doi: 10.1109/ICCICC46617.2019.9146101.
[14] R. Kosuru, Z. Qu, Z. Ding, and P. Moo, "A modified reinforcement Q-learning method for multi-function phased array radar beam scheduling," in *Proc. IEEE 21st Int. Conf. Cognit. Informat. Cognit. Comput. (ICCI*CC)*, Dec. 2022, pp. 16–21, doi: 10.1109/ICCICC57084.2022.10101623.
[15] J. Qin, M. Zhu, Z. Pan, Y. Li, and Y. Li, "Memory-based deep reinforcement learning for cognitive radar target tracking waveform resource management," *IET Radar, Sonar Navigat.*, vol. 17, no. 12, pp. 1822–1836, Dec. 2023, doi: 10.1049/rsn2.12469.
[16] S. Akbar, R. S. Adve, Z. Ding, and P. W. Moo, "Task scheduling in cognitive multifunction radar using model-based DRL," *IEEE Trans. Aerosp. Electron. Syst.*, vol. 61, no. 2, pp. 2434–2449, Apr. 2025, doi: 10.1109/TAES.2024.3475991.
[17] I. Mallioras, Z. D. Zaharis, P. I. Lazaridis, and S. Pantelopoulos, "A novel realistic approach of adaptive beamforming based on deep neural networks," *IEEE Trans. Antennas Propag.*, vol. 70, no. 10, pp. 8833–8848, Oct. 2022, doi: 10.1109/TAP.2022.3168708.
[18] Y.-D. Lin, J.-H. Chang, and Y.-C. Lai, "Deep reinforcement learning-based adaptive nulling in phased array under dynamic environments," *IEEE Access*, vol. 13, pp. 130988–131002, 2025, doi: 10.1109/ACCESS.2025.3591643.
[19] P. Ramezanpour, M. J. Rezaei, and M. R. Mosavi, "Deep-learning-based beamforming for rejecting interferences," *IET Signal Process.*, vol. 14, no. 7, pp. 467–473, Sep. 2020, doi: 10.1049/iet-spr.2019.0495.
[20] P. Ramezanpour and M.-R. Mosavi, "Two-stage beamforming for rejecting interferences using deep neural networks," *IEEE Syst. J.*, vol. 15, no. 3, pp. 4439–4447, Sep. 2021, doi: 10.1109/JSYST.2020.3034957.
[21] S. Mohammadzadeh, V. H. Nascimento, R. C. de Lamare, and N. Hajarolasvadi, "Robust beamforming based on complex-valued convolutional neural networks for sensor arrays," *IEEE Signal Process. Lett.*, vol. 29, pp. 2108–2112, 2022, doi: 10.1109/LSP.2022.3212637.
[22] J. Lim, H. Yoo, E. Lee, S. Oh, and J. Lee, "Robust anti-jamming method for large-array radar systems using deep learning based null-space beamforming," *IEEE Access*, vol. 13, pp. 103599–103612, 2025, doi: 10.1109/ACCESS.2025.3579422.
[23] J. Chen, J. Tao, S. Luo, S. Li, C. Zhang, and W. Xiang, "A deep learning driven hybrid beamforming method for millimeter wave MIMO system," *Digit. Commun. Netw.*, vol. 9, no. 6, pp. 1291–1300, Dec. 2023, doi: 10.1016/j.dcan.2022.07.005.
[24] K. Ikeagu, M. R. A. Khandaker, C. Song, and Y. Ding, "Deep learning-based hybrid beamforming design for IRS-aided MIMO communication," *IEEE Wireless Commun. Lett.*, vol. 13, no. 2, pp. 461–465, Feb. 2024, doi: 10.1109/LWC.2023.3332016.
[25] S. Lv, X. Li, T. Fan, J. Liu, and M. Shi, "Deep learning-based overhead minimizing hybrid beamforming for wideband mmWave systems," *IEEE Wireless Commun. Lett.*, vol. 11, no. 7, pp. 1389–1393, Jul. 2022, doi: 10.1109/LWC.2022.3170597.
[26] S. Shi, Y. Cai, Q. Hu, B. Champagne, and L. Hanzo, "Deep-unfolding neural-network aided hybrid beamforming based on symbol-error probability minimization," *IEEE Trans. Veh. Technol.*, vol. 72, no. 1, pp. 529–545, Jan. 2023, doi: 10.1109/TVT.2022.3201961.
[27] Y. Arjoune and S. Faruque, "Experience-driven learning-based intelligent hybrid beamforming for massive MIMO mmWave communications," *Phys. Commun.*, vol. 51, Apr. 2022, Art. no. 101534, doi: 10.1016/j.phycom.2021.101534.
[28] Y. Li, Y. Lu, G. Zhang, B. Ai, D. Niyato, and S. Cui, "Homogeneous and heterogeneous graph learning for hybrid beamforming in mmWave systems," *IEEE Trans. Wireless Commun.*, vol. 24, no. 10, pp. 8086–8100, Oct. 2025, doi: 10.1109/TWC.2025.3564290.
[29] Q. Wang, X. Li, S. Jin, and Y. Chen, "Hybrid beamforming for mmWave MU-MISO systems exploiting multi-agent deep reinforcement learning," *IEEE Wireless Commun. Lett.*, vol. 10, no. 5, pp. 1046–1050, May 2021, doi: 10.1109/LWC.2021.3056702.
[30] H. Hojatian, J. Nadal, J.-F. Frigon, and F. Leduc-Primeau, "Unsupervised deep learning for massive MIMO hybrid beamforming," *IEEE Trans. Wireless Commun.*, vol. 20, no. 11, pp. 7086–7099, Nov. 2021, doi: 10.1109/TWC.2021.3080672.
[31] Y. Zhang, T. Osman, and A. Alkhateeb, "Online beam learning with interference nulling for millimeter wave MIMO systems," *IEEE Trans. Wireless Commun.*, vol. 23, no. 5, pp. 5109–5124, May 2024, doi: 10.1109/TWC.2023.3324621.
[32] L. Xu, S. Sun, Y. D. Zhang, and A. P. Petropulu, "Reconfigurable beamforming for automotive radar sensing and communication: A deep reinforcement learning approach," *IEEE J. Sel. Areas Sensors*, vol. 1, pp. 124–138, 2024, doi: 10.1109/JSAS.2024.3431462.



JAEHYUK LIM (Member, IEEE) received the B.S. degree in computer and communication engineering and the Ph.D. degree in computer and radio communications engineering from Korea University, Seoul, South Korea, in 2014 and 2020, respectively. From 2020 to 2025, he was a Senior Researcher with the Agency for Defense Development (ADD), focusing on smart radar systems, including array antennas and signal processing. Since 2026, he has been with ETRI. His research interests include integrated sensing and communication systems (ISAC) and AI-based signal processing.



SEUNGHYUN JANG (Member, IEEE) received the M.S. and Ph.D. degrees in electrical engineering from Korea Advanced Institute of Science and Technology (KAIST), Daejeon, South Korea, in 2003 and 2017, respectively. Since 2003, he has been with the Electronics and Telecommunications Research Institute (ETRI), South Korea, where he is currently the Director of the RF Technology Research Section. His recent research interests include integrated sensing and communication (ISAC), sub-band full-duplex, and surface-wave communication technologies.



HOGEUN YOO received the B.S. degree from G-TEC and the M.S. degree in computer science from Korea University, Seoul, South Korea, where he is currently pursuing the Ph.D. degree. His research interests include artificial intelligence, optimization, and antenna array problems.



JAEHOON LEE received the B.S. degree in radio engineering from Korea University, Seoul, South Korea, in 1997, the M.S. degree in electrical engineering from Korea Advanced Institute of Science and Technology, Taejon, South Korea, in 1999, and the Ph.D. degree in radio engineering from Korea University, in 2003. From 2003 to 2008, he was with the Telecommunication Research and Development Center, Telecommunication Network Business Division, Samsung Electronics, Suwon, South Korea. He is currently a Professor with the Department of Computer Science and Engineering, Korea University. His current research interests include modeling and simulation of optical and microwave components, signal processing, and high-speed digital transmission systems.